Advances in Computational Design, *Vol. 5, No. 2 (2020) 177-193*
DOI: https://doi.org/10.12989/acd.2020.5.2.177

Finite element based modeling and thermal dynamic analysis of functionally graded graphene reinforced beams

Ammar F.H. Al-Maliki, Ridha A. Ahmed, Nader M. Moustafa and Nadhim M. Faleh*

Al-Mustansiriah University, Engineering Collage P.O. Box 46049, Bab-Muadum, Baghdad 10001, Iraq

(Received September 29, 2019, Revised November 13, 2019, Accepted November 17, 2019)

Abstract. In the present research, dynamic analysis of functionally graded (FG) graphene-reinforced beams under thermal loading has been carried out based on finite element approach. The presented formulation is based on a higher order refined beam element accounting for shear deformations. The graphene-reinforced beam is exposed to transverse periodic mechanical loading. Graphene platelets have three types of dispersion within the structure including uniform-type, linear-type and nonlinear-type. Convergences and validation studies of derived results from finite element approach are also presented. This research shows that the resonance behavior of a nanocomposite beam can be controlled by the GPL content and dispersions. Therefore, it is showed that the dynamical deflections are notably influenced by GPL weight fractions, types of GPL distributions, temperature changes, elastic foundation and harmonic load excitation frequency.

Keywords: finite element method; thermal load; refined beam element; graphene platelet; dynamic loading

1. Introduction

In recent decades, several carbon based structures containing carbon nanotube or carbon fiber have been widely utilized in composites for enhancing their mechanics and thermal specifications (Zhang 2017, Keleshtreri *et al*. 2016). A 273% enhancement of elastic modulus is obtained by Ahankari *et al*. (2010) for carbon reinforced composites in comparison to conventional composites. Likewise, Gojny *et al*. (2004) mentioned that structural stiffness of carbon based composites may be enhanced with incorporation of carbon nanotube within material. Impacts of configuration and scale of carbon nanotubes on rigidity growth of material composites having metallic matrices are studied by Esawi *et al*. (2011). Because of possessing above mentioned properties, beam and plate structures having carbon based fillers are researched to understand their static or dynamical status (Yang *et al*. 2017). There are also some investigations on composite or functionally graded materials and interested readers are refaced to new investigations on materials (Barati and Zenkour 2018, She *et al*. 2018, 2019). Furthermore, the graphene based composite material has been recently gained enormous attentions because of having easy producing procedure and high rigidity growth. Nieto *et al*. (2017) presented a review paper based on several graphene based composite material possessing ceramic or metallic matrices. The multi-scale study

*Corresponding author, Professor, E-mail: dr.nadhim@uomustansiriyah.edu.iq

http://www.techno-press.org/?journal=acd&subpage=7 ISSN: 2383-8477 (Print), 2466-0523 (Online)

of mechanical attributes for graphene based composite material has been provided by Lin *et al*. (2018) utilizing finite elements approach.

Until now, many of researches in the fields of nano-composites have been interested in production and materials characteristics recognition of graphene based composites and structural components containing slight percentages of graphene fillers. For instance, it is mentioned by Rafiee *et al*. (2009) that some material characteristics of graphene based composites may be enhanced via placing 0.1% volume of graphene filler. However, achieving to this level of reinforcement employing nanotubes required 1% of their volume. Graphene based composites containing epoxy matrix were created by King *et al*. (2013) by placing 6% weight fraction of graphene fillers to polymeric phases. It was stated that Young modulus of the composite has been increased from 2.72 GPa to 3.36 GPa. Next, 57% increment for Young modulus has been achieved by Fang *et al*. (2009) based on a sample of graphene based composite.

Moreover, many studies in the fields of nano-mechanic are associated with vibrational and stability investigation of various structural elements containing beam or plate reinforced via diverse graphene dispersions. For instance, vibrational properties of a laminated graphene based plate have been explored by Song *et al*. (2017) assuming simply support edge condition. They assumed that the plate is constructed from particular numbers of layers each containing a sensible content of graphene. Selecting a perturbation approach, static deflections and bucking loads of graphene based plates have been derived by Shen *et al*. (2017). In above papers, each material property has discontinuous variation across the thickness of beam or plate. Also, geometrically nonlinear vibration frequencies of graphene based beams having embedded graphene have been explored by Feng *et al*. (2017) selecting first-order beam theory. Moreover, vibration frequencies of graphene based beams having porosities have been explored by Kitipornchai *et al*. (2017).

This paper is devoted to analyze mechanical-thermal dynamic behavior of a macro-size beam reinforced with graphene platelets (GPLs) based on finite element approach. Graphene platelets have three types of dispersion within the structure including uniform-type, linear-type and nonlinear-type. The presented formulation is based on a higher order refined beam element accounting for shear deformations. So, it is useful for thick beams. The graphene-reinforced beam is exposed to transverse periodic mechanical loading. Via finite element procedure, forced vibration path of the beam has been derived. It will be demonstrated that dynamic characteristics of the graphene-reinforced beam are dependent on geometric amplitude, thermal loading, graphene distribution and amount.

2. Graphene based composites

According to Fig.1, it is assumed that graphene platelets have three types of dispersion within the structure including uniform-type, linear-type and nonlinear-type. According to Fig.2, a graphene reinforced composite micro-scale beam is illustrated. Micro-mechanic theory of such composite materials (Liew *et al*. 2015) introduces the below relationship between graphene platelets weight fraction (W_{GPL}) and their volume fraction (V_{GPL}) by:

$$V_{GPL} = \frac{W_{GPL}}{W_{GPL} + \frac{\rho_{GPL}}{\rho_M} - \frac{\rho_{GPL}}{\rho_M} W_{GPL}} \tag{1}$$

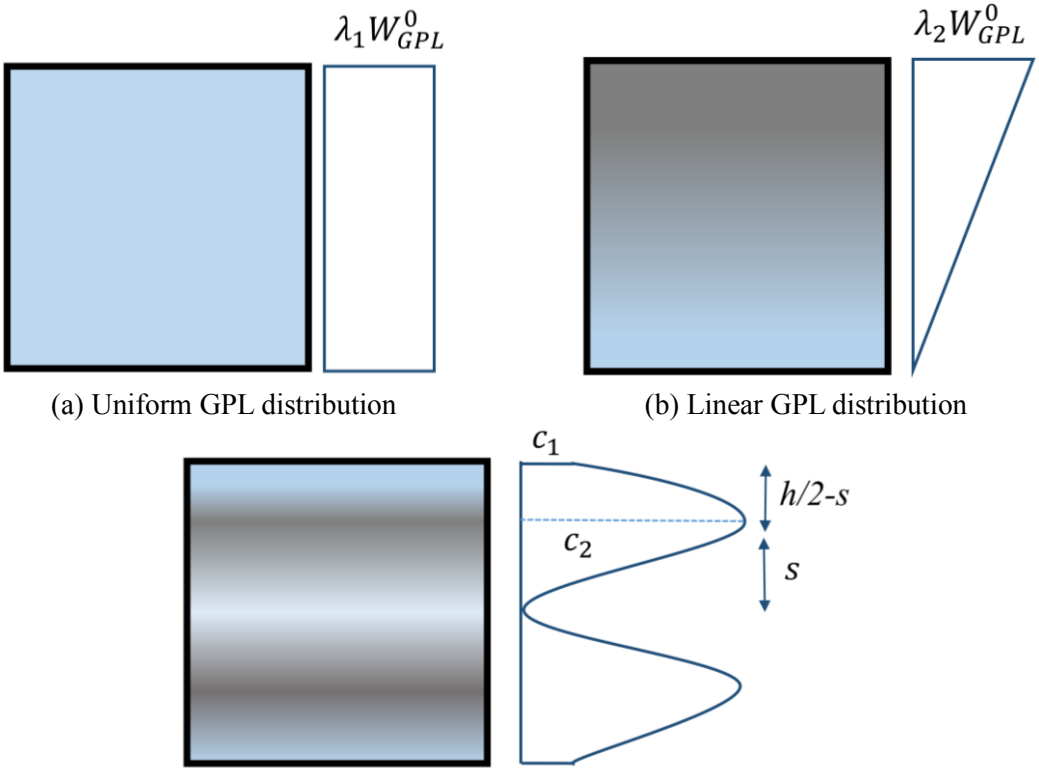

(a) Uniform GPL distribution (b) Linear GPL distribution

(c) Nonlinear GPL distribution

Fig. 1 GPL dispersions in the thickness direction

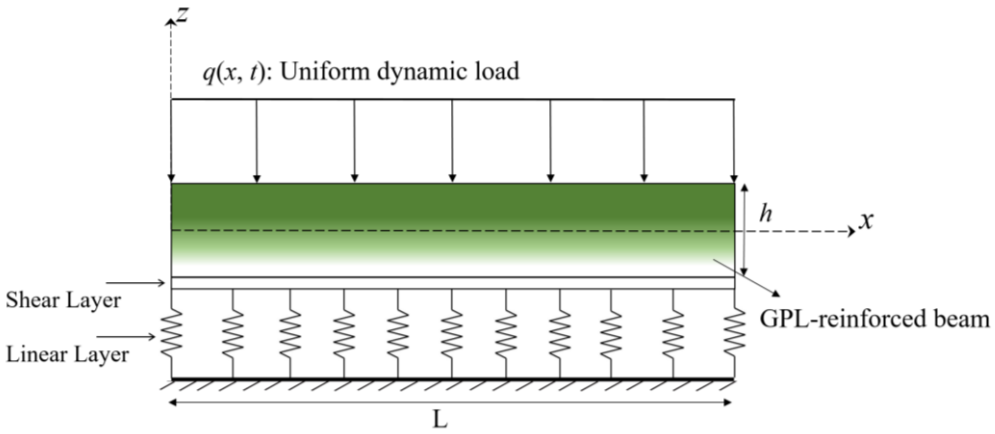

Fig. 2 Geometry and coordinates of GPL-reinforced beam

where ρ_{GPL} and ρ_M define the mass densities of graphene and polymeric matrices, respectively. Next, the elastic modulus of a graphene based composite might be represented based upon matrix elastic modulus (E_M) by:

$$E_1 = \frac{3}{8}\left(\frac{1+\xi_L^{GPL}\eta_L^{GPL}V_{GPL}}{1-\eta_L^{GPL}V_{GPL}}\right)E_M + \frac{5}{8}\left(\frac{1+\xi_W^{GPL}\eta_W^{GPL}V_{GPL}}{1-\eta_W^{GPL}V_{GPL}}\right)E_M \tag{2}$$

so that ξ_L^{GPL} and ξ_W^{GPL} define two geometrical factors indicating the impacts of graphene configuration and scales as:

$$\xi_L^{GPL} = \frac{2l_{GPL}}{t_{GPL}} \tag{3a}$$

$$\eta_L^{GPL} = \frac{\left(E_{GPL}/E_M\right)-1}{\left(E_{GPL}/E_M\right)+\xi_L^{GPL}} \tag{3b}$$

$$\xi_W^{GPL} = \frac{2w_{GPL}}{t_{GPL}} \tag{3c}$$

$$\eta_W^{GPL} = \frac{\left(E_{GPL}/E_M\right)-1}{\left(E_{GPL}/E_M\right)+\xi_W^{GPL}} \tag{3d}$$

so that w_{GPL} , l_{GPL} , and t_{GPL} define platelets average widths, length, and thickness, respectively. Furthermore, Poisson's ratio for graphene based composite might be defined based upon Poisson's ratio of the two constituents in the form:

$$\begin{aligned} \nu_1 &= \nu_{GPL}V_{GPL} + \nu_M V_M \\ \alpha_1 &= \alpha_{GPL}V_{GPL} + \alpha_M V_M \end{aligned} \tag{4}$$

in which $V_M = 1 - V_{GPL}$ expresses the volume fractions of matrix component. Herein, three dispersions of the platelets have been assumed as:

Uniform:

$$W_{GPL} = \lambda_1 W_{GPL}^0 \tag{5a}$$

Linear:

$$W_{GPL} = \lambda_2 W_{GPL}^0 \left(\frac{z}{h} + \frac{1}{2}\right) \tag{5b}$$

Nonlinear:

$$W_{GPL} = \frac{\lambda_3 W_{GPL}^0 z^2}{s^2 h^2 (4s^2 - h^2)}\left[4h^2 z^2 - h^4 + \frac{16s^2}{n}(s^2 - z^2)\right] \tag{5c}$$

where $W_{GPL}^0 = 1\%$ expresses a particular weight fraction for graphene platelets.

3. Beam modeling via refined theory

With the employment of refined beam theory, a displacement field having following forms might be expressed to start mathematical modeling of the beam (Barati 2017, Mouffoki *et al*. 2017, Fenjan *et al*. 2019, Ahmed *et al*. 2019, Zemri *et al*. 2015, Bounouara *et al*. 2016):

$$u_x(x,z,t) = u_0(x,t) - z\frac{\partial w_b}{\partial x} - f(z)\frac{\partial w_s}{\partial x} \tag{6a}$$

$$u_y(x,z,t) = 0 \tag{6b}$$

$$u_z(x,z,t) = w_b(x,t) + w_s(x,t) \tag{6c}$$

Here u ; w_b and w_s express the axial and transverse field coefficients.

For the refined beam model, the strain field might be expressed by (Ahmed *et al*. 2019):

$$\epsilon_x = \frac{\partial u_0}{\partial x} - z\frac{\partial^2 w_b}{\partial x^2} - f(z)\frac{\partial^2 w_s}{\partial x^2} \tag{7a}$$

$$\epsilon_y = \epsilon_z = \gamma_{xy} = \gamma_{yz} = 0 \tag{7b}$$

$$\gamma_{xz} = 2\epsilon_{xz} = g(z)\frac{\partial w_s}{\partial x} \tag{7c}$$

where $f(z) = z - h\sinh(\frac{z}{h}) + z\cosh(\frac{1}{2})$ and $g(z) = 1 - f'(z)$.

To derive weak formulation required for finite element method, first it is necessary to express the Hamiltonian of a dynamic system as: $\mathrm{H} = U - V - K$.

Here U is strain energy and K is kinetic energy. The strain energy can be stated as (Faleh *et al*. 2018, She *et al*. 2018):

$$\begin{aligned} U &= 0.5\int_0^L \int_{-\frac{h}{2}}^{\frac{h}{2}} \left(\sigma_{ij}\delta\epsilon_{ij}\right) dz dx \\ &= \int_0^L \int_{-\frac{h}{2}}^{\frac{h}{2}} (\sigma_x \delta\epsilon_x + \tau_{xz}\delta\gamma_{xz}) dz dx = \int_0^L \Bigg(A_{11}\frac{du_0}{dx}\frac{du_0}{dx} - 2B_{11}\frac{du_0}{dx}\frac{d^2w_b}{dx^2} \\ &+ D_{11}\frac{d^2w_b}{dx^2}\frac{d^2w_b}{dx^2} - 2B_{11}^s\frac{du_0}{dx}\frac{d^2w_s}{dx^2} - (2D_{11}^s + 0.5 * (A^s))\frac{d^2w_b}{dx^2}\frac{d^2w_s}{dx^2} \\ &+ H_{11}^s \Bigg) dx \end{aligned} \tag{8}$$

where A_{11} , B_{11}^s , etc., are the beam stiffness, defined by:

$$(A_{11}, B_{11}, D_{11}, B_{11}^{s}, D_{11}^{s}, H_{11}^{s}) = \int_{-\frac{h}{2}}^{\frac{h}{2}} E(z)(1, z, z^2, f, zf, f^2)dz \tag{9}$$

$$A^{s} = \int_{-\frac{h}{2}}^{\frac{h}{2}} G(z)g^2 dz \tag{10}$$

The kinetic energy of beam is written as:

$$\begin{aligned} K &= \int_0^L \int_{-\frac{h}{2}}^{\frac{h}{2}} \rho(z)[\dot{u}_x\dot{u}_x + \dot{u}_y\dot{u}_y]\, dzdx \\ &= \int_0^L \Big\{ I_0[\dot{u}_0\dot{u}_0 + (\dot{w}_b + \dot{w}_s)(\dot{w}_b + \dot{w}_s)] - 2[I_1\left(\dot{u}_0 \frac{d\dot{w}_b}{dx}\right)] + I_2[\left(\frac{d\dot{w}_b}{dx}\frac{d\dot{w}_b}{dx}\right)] \\ &\quad - 2J_1[\left(\dot{u}_0 \frac{d\dot{w}_s}{dx}\right)] + K_2[\left(\frac{d\dot{w}_s}{dx}\frac{d\dot{w}_s}{dx}\right)] + 2J_2[\left(\frac{d\dot{w}_b}{dx}\frac{d\dot{w}_s}{dx}\right)]\Big\} dx \end{aligned} \tag{11}$$

in which dot-superscript denote the differentiation with respect to the time variable *t;* and the mass inertias are expressed as:

$$(I_0, I_1, J_1, I_2, J_2, K_2) = \int_{-\frac{h}{2}}^{\frac{h}{2}} (1, z, f, z^2, zf, f^2)\rho(z)dz \tag{12}$$

Also, the work done by the external applied forces can be expressed as:

$$V = 0.5\int_0^L [(k_p - N^T)(\frac{\partial(w_b + w_s)}{\partial x}\frac{\partial(w_b + w_s)}{\partial x} - k_w(w_b + w_s) + q(w_b + w_s)]dx \tag{13}$$

where k_w and k_p are Winkler and Pasternak constants; $q_{dynamic}$ is applied transverse dynamic load and N^T is in-plane thermal loading: $N^T = \int_{-h/2}^{h/2} E_1 \alpha_1 (T - T_0)\, dz$; $T = \Delta T(\frac{z}{h} + 0.5) + T_0$ and ΔT is temperature rise. In the present paper, the linear temperature rise has been adopted.

4. Method of finite elements

Through the present section, the method of finite elements has been selected for solving the dynamical problem of a graphene based beam having S-S and C-C edges. For this goal, the refined beam element has been used with ten degrees of freedom indicated in Fig.3. Herein, a shape

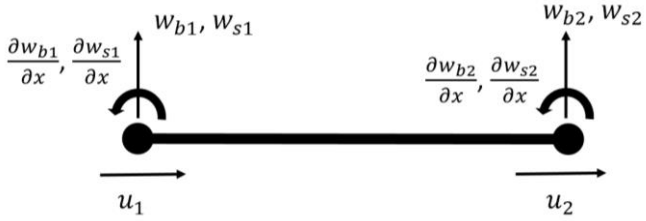

Fig. 3 Degrees of freedom for the refined master element

function has been introduced for axial field component, and also Hermit shape function have been introduced for lateral field components which are:

$$u_0(x,t) = \sum_{i=1}^{2} U_i(t) N_i(x) = N_1 U_1 + N_2 U_2 \tag{14}$$

$$w_b(x,t) = \sum_{i=1}^{4} W_{bi}(t) \tilde{N}_i(x) = \tilde{N}_1 W_{b1} + \tilde{N}_2 W'_{b1} + \tilde{N}_3 W_{b2} + \tilde{N}_4 W'_{b2} \tag{15}$$

$$w_s(x,t) = \sum_{i=1}^{4} W_{si}(t) \tilde{N}_i(x) = \tilde{N}_1 W_{s1} + \tilde{N}_2 W'_{s1} + \tilde{N}_3 W_{s2} + \tilde{N}_4 W'_{s2} \tag{16}$$

So that U_i , W_{bi} and W_{si} are field coefficients and shape functions are:

$$N_1 = 1 - \frac{x}{L_e} \tag{17}$$

$$N_2 = \frac{x}{L_e} \tag{18}$$

$$\tilde{N}_1 = \frac{1}{L_e^3}\left(2x^3 - 3x^2 L_e + L_e^3\right) \tag{19}$$

$$\tilde{N}_2 = \frac{1}{L_e^3}\left(x^3 L_e - 2x^2 L_e^2 + x L_e^3\right) \tag{20}$$

$$\tilde{N}_3 = \frac{1}{L_e^3}\left(-2x^3 + 3x^2 L_e\right) \tag{21}$$

$$\tilde{N}_4 = \frac{1}{L_e^3}\left(x^3 L_e - x^2 L_e^2\right) \tag{22}$$

so that L_e defines the length for master element.

Placing Eqs. (8)-(13) in Hamiltonian and minimizing it to field coefficients U_i, W_{bi}, and W_{si} (Rezaiee-Pajand *et al*. 2018, Al-Maliki *et al*. 2019) results in below relation containing simultaneous algebraic equations:

$$\frac{\partial H}{\partial U_i}=\frac{\partial H}{\partial W_{bi}}=\frac{\partial H}{\partial W_{si}}=0 \tag{23}$$

Next, the solution trend yields:

$$\left\{\begin{pmatrix}[k_{11}] & [k_{12}] & [k_{13}]\\ [k_{21}] & [k_{22}] & [k_{23}]\\ [k_{31}] & [k_{32}] & [k_{33}]\end{pmatrix}_{10*10}+\omega_{ex}{}^2\begin{pmatrix}[m_{11}] & [m_{12}] & [m_{13}]\\ [m_{21}] & [m_{22}] & [m_{23}]\\ [m_{31}] & [m_{32}] & [m_{33}]\end{pmatrix}_{10*10}\right\}\begin{Bmatrix}U_i\\ W_{bi}\\ W_{si}\end{Bmatrix}=\begin{Bmatrix}0\\ F_1\\ F_1\end{Bmatrix} \tag{24}$$

so that k_{ij} and m_{ij} define stiffness and mass matrices for master element, respectively; F_1 defines exerted dynamical loading to master element. Obtained system may be solved for deriving transverse center deflections of a beam $W=W_b+W_s$ as a function of external frequency ω_{ex}. Based on adequate numbers of beam element, it is feasible to reach the exact solutions.

Next, normalized factors may be selected by:

$$\Omega=\omega_{ex}L^2\sqrt{\frac{\rho_M A}{\mathrm{E}_M I}},\ K_w=\frac{k_w L^4}{E_M I},K_p=\frac{k_p L^2}{E_M I} \tag{25}$$

All components for mass and stiffness matrices together with load vector achieved by Eq.(23) have been introduced as:

$$k_{11}=A_{11}\int_0^{L_e}\frac{\partial N_i}{\partial x}\frac{\partial N_j}{\partial x}dx$$

$$k_{12}=-B_{11}\int_0^{L_e}\frac{\partial N_i}{\partial x}\frac{\partial^2\tilde{N}_j}{\partial x^2}dx,\ \ k_{21}=-B_{11}\int_0^{L_e}\frac{\partial N_j}{\partial x}\frac{\partial^2\tilde{N}_i}{\partial x^2}dx$$

$$k_{22}=D_{11}\int_0^{L_e}\frac{\partial^2\tilde{N}_i}{\partial x^2}\frac{\partial^2\tilde{N}_j}{\partial x^2}dx-k_w\int_0^{L_e}\tilde{N}_i\tilde{N}_j dx+(k_p-N^T)\int_0^{L_e}\frac{\partial\tilde{N}_i}{\partial x}\frac{\partial\tilde{N}_j}{\partial x}dx$$

$$k_{13}=-B_{11}^s\int_0^{L_e}\frac{\partial N_i}{\partial x}\frac{\partial^2\tilde{N}_j}{\partial x^2}dx,\ \ k_{31}=-B_{11}^s\int_0^{L_e}\frac{\partial N_j}{\partial x}\frac{\partial^2\tilde{N}_i}{\partial x^2}dx \tag{26}$$

$$k_{23}=-D_{11}^s\int_0^{L_e}\frac{\partial^2\tilde{N}_i}{\partial x^2}\frac{\partial^2\tilde{N}_j}{\partial x^2}dx-k_w\int_0^{L_e}\tilde{N}_i\tilde{N}_j dx+(k_p-N^T)\int_0^{L_e}\frac{\partial\tilde{N}_i}{\partial x}\frac{\partial\tilde{N}_j}{\partial x}dx$$

$$k_{33}=H_{11}^s\int_0^{L_e}\frac{\partial^2\tilde{N}_i}{\partial x^2}\frac{\partial^2\tilde{N}_j}{\partial x^2}dx+A^s\int_0^{L_e}\frac{\partial^2\tilde{N}_i}{\partial x^2}\frac{\partial^2\tilde{N}_j}{\partial x^2}dx$$

$$-k_w\int_0^{L_e}\tilde{N}_i\tilde{N}_j dx+(k_p-N^T)\int_0^{L_e}\frac{\partial\tilde{N}_i}{\partial x}\frac{\partial\tilde{N}_j}{\partial x}dx$$

$$m_{11} = I_0 \int_0^{L_e} N_i N_j dx$$

$$m_{22} = I_0 \int_0^{L_e} \tilde{N}_i \tilde{N}_j dx + I_2 \int_0^{L_e} \frac{\partial \tilde{N}_i}{\partial x} \frac{\partial \tilde{N}_j}{\partial x} dx$$

$$m_{12} = -I_1 \int_0^{L_e} N_i \frac{\partial \tilde{N}_j}{\partial x} dx, \quad m_{21} = -I_1 \int_0^{L_e} N_j \frac{\partial \tilde{N}_i}{\partial x} dx$$

$$m_{13} = -J_1 \int_0^{L_e} N_i \frac{\partial \tilde{N}_j}{\partial x} dx, \quad m_{31} = -J_1 \int_0^{L_e} N_j \frac{\partial \tilde{N}_i}{\partial x} dx$$

$$m_{23} = J_2 \int_0^{L_e} \frac{\partial \tilde{N}_i}{\partial x} \frac{\partial \tilde{N}_j}{\partial x} dx$$

$$m_{33} = I_0 \int_0^{L_e} \tilde{N}_i \tilde{N}_j dx + K_2 \int_0^{L_e} \frac{\partial \tilde{N}_i}{\partial x} \frac{\partial \tilde{N}_j}{\partial x} dx$$

$$F_i = \int_0^{L_e} q_{dynamic} \tilde{N}_i dx$$

Table 1 Gradient index effects on total content of graphene

Uniform (λ_1)	Linear (λ_2)	Nonlinear (λ_3)	$\%W^*_{GPL}$
0	0	0	0
0.33	0.67	0.43	0.33
1	2	1.29	1

Table 2 Material and geometrical factors for graphene based beams

GPLs	Matrix (Epoxy resin)
E_{GPL}=1.01 TPa	E_M=2.85 GPa
ρ_{GPL}=1062.5 kg/m^3	ρ_M=1200 kg/m^3
v_{GPL}=0.006	v_M=0.34
α_{GPL}=2.35× $10^{-5}/K$	α_M=8.2× $10^{-5}/K$
t_{GPL}=1.5 nm	-
w_{GPL}=1.5 μm	-
l_{GPL}=2.5 μm	-

5. Graphical results and discussions

In the present section, dynamic analysis of functionally graded (FG) graphene-reinforced beams under thermal loading has been carried out based on finite element approach. The presented

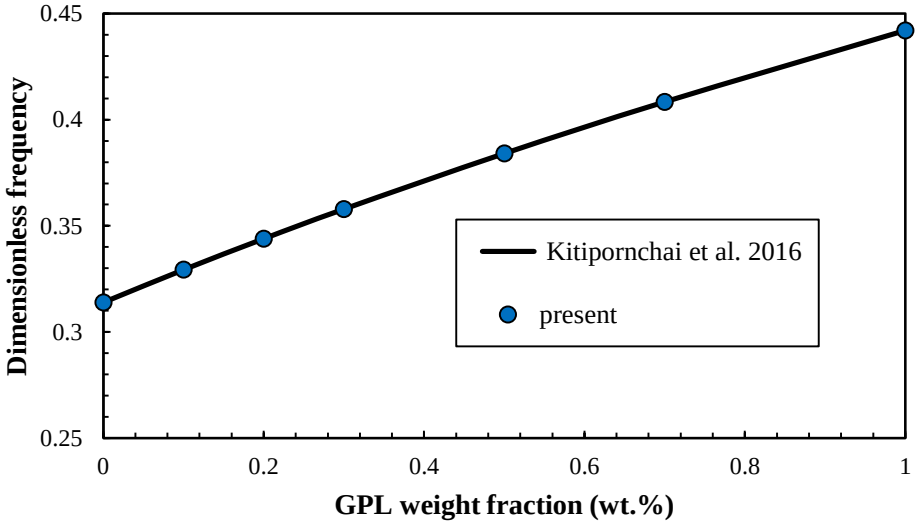

Fig. 4 Validation of the dimensionless vibration frequency of GPL-reinforced beams (L/h=20)

Table 3 Convergence of the vibrational frequency of uniformly graphene based beam (L/h=10, W^*_{GPL}=1%)

Elements number	S-S	C-C
2	20.8610	47.5977
3	20.7961	47.0170
4	20.7846	46.8766
5	20.7814	46.8328
10	20.7794	46.7934
12	20.7793	46.7901
15	20.7792	46.7872
20	20.7792	46.7848
25	20.7792	46.7836
30	20.7792	46.7830
35	20.7792	46.7830

formulation was based on a higher order refined beam element accounting for shear deformations. The graphene-reinforced beam is exposed to transverse periodic mechanical loading. Graphene platelets have three types of dispersion within the structure including uniform-type, linear-type and nonlinear-type. Tables 1 and 2 provide excellent information about material properties.

The convergences and verifications of proposed approach have been respectively represented by Table 3 and Fig.4. Based upon Table 3, one can deduce that vibrational frequencies are converged via selecting fifteen elements for S-S beams and thirty elements for C-C beams. The number of elements have been adopted for presented investigation in this article. Furthermore, Fig.4 depicts that achieved frequency for graphene based beams are identical to those represented by Kitipornchai *et al*. (2016) based upon different graphene weight fractions.

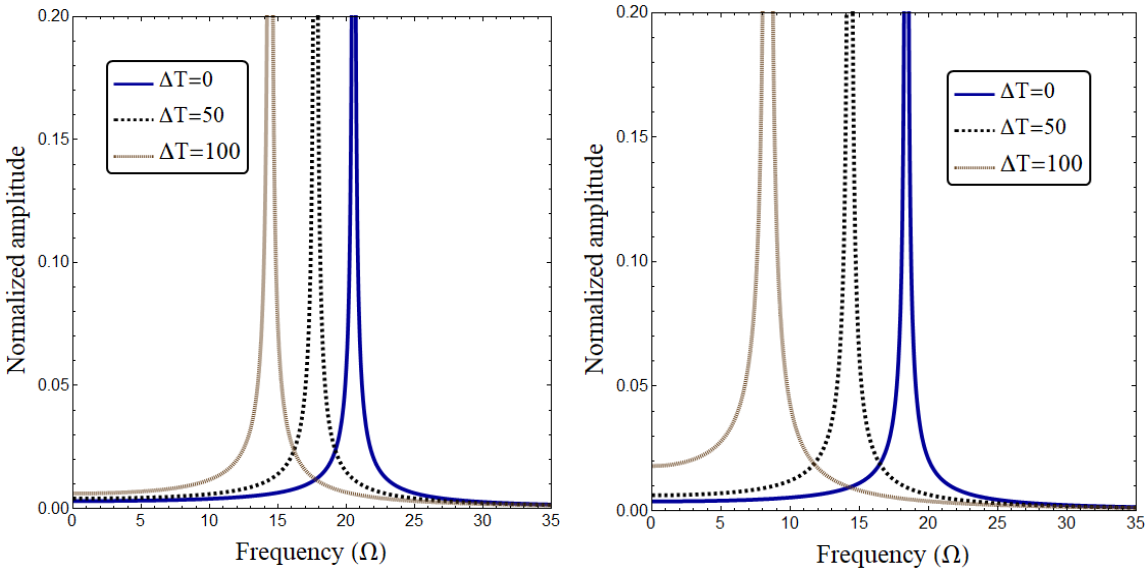

(a) Uniform GPL distribution (b) Linear GPL distribution

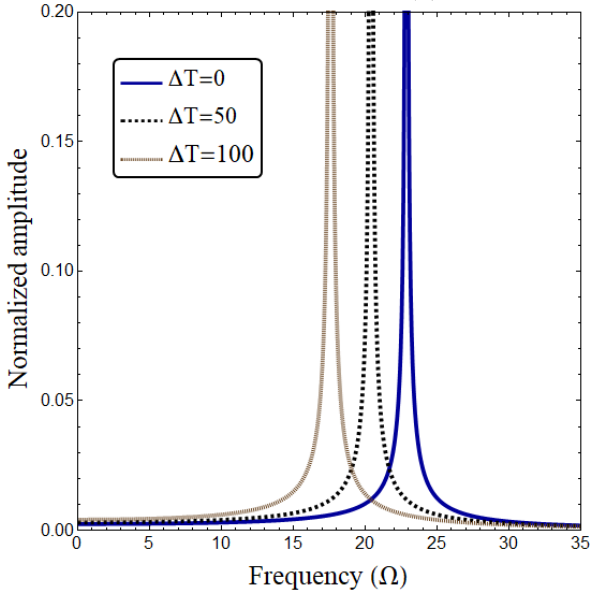

(c) Nonlinear GPL distribution

Fig. 5 Dynamical deflections of graphene based beams versus external frequency for different graphene distributions and temperature changes (L/h=10, K_w=0, K_p=0, W^*_{GPL}=1%)

Dynamical deflections of graphene based beams with respect to external frequency based on different graphene dispersions and temperatures have been depicted in Fig.5 when L =10h and W^*_{GPL}=1%. The graphene based beam has been assumed as simply-supported at left and right

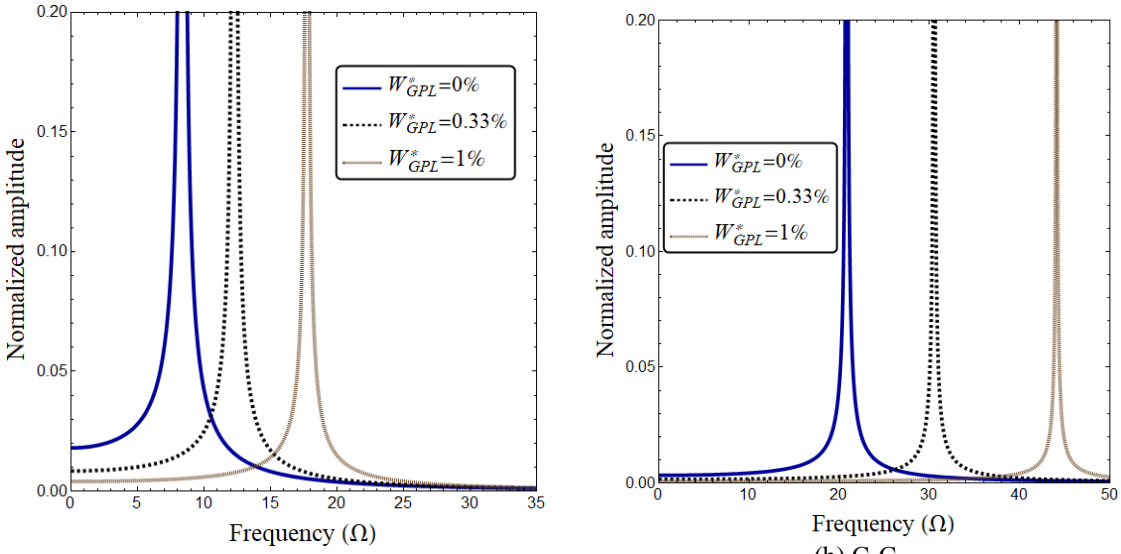

(a) S-S (b) C-C

Fig. 6 Dynamical deflections of graphene based beams versus external frequency for different uniform graphene weight fractions and boundary conditions (L/h=10, K_w=0, K_p=0, ΔT=50)

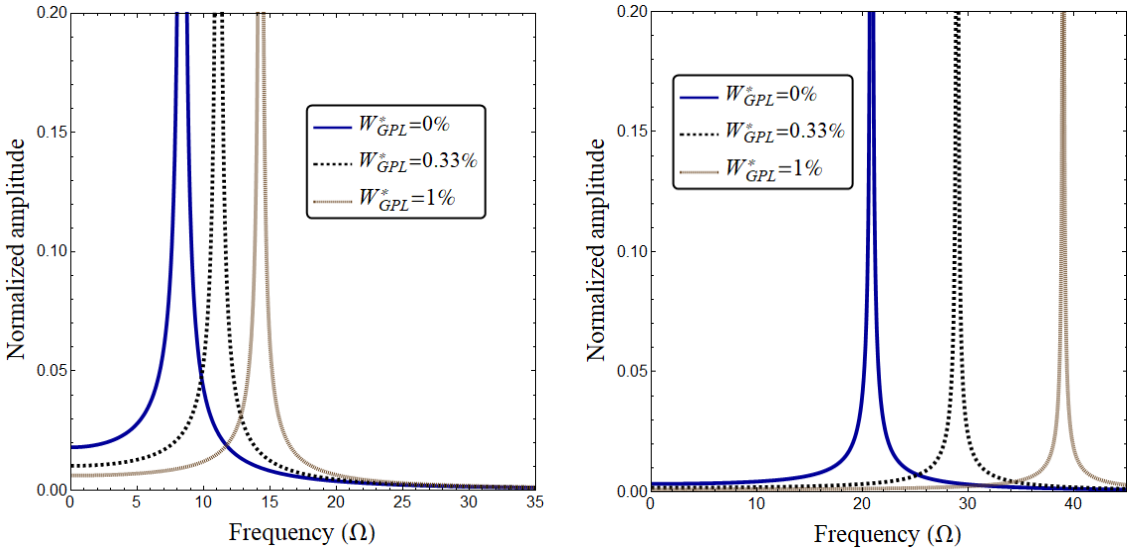

(a) S-S (b) C-C

Fig. 7 Dynamical deflections of graphene based beams versus external frequency for different linear graphene weight fractions and boundary conditions (L/h=10, K_w=0, K_p=0, ΔT=50)

edges. Firstly, it is better to express that this graph illustrates normalized deflection as a function of external frequency of exerted harmonic mechanical load. This means that at a particular value of the external frequency the resonance phenomena together with large deflections may be observed. It is well known that the beam structural rigidity will be reduced via linear temperature rise. Accordingly, the forced vibration curves will move to the left highlighting smaller resonance

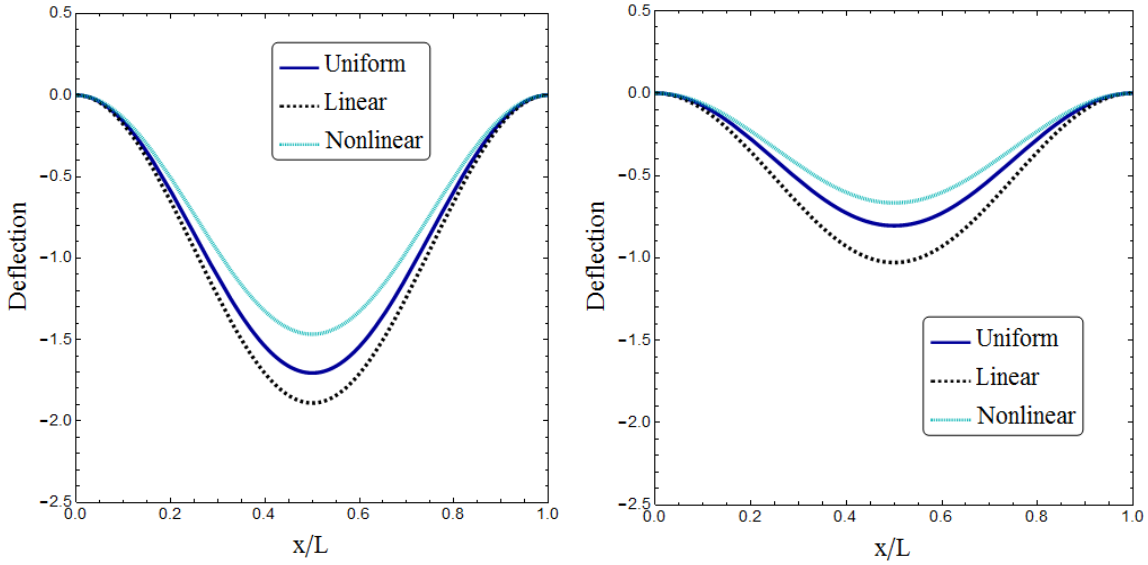

(a) W^*_{GPL}=0.33 (b) W^*_{GPL}=1

Fig. 8 First mode shape of C-C nano-composite beam for various GPL distributions (L/h=10, K_w=0, K_p=0, Ω=5, ΔT=50)

frequency. Furthermore, linear temperature rise impacts are dependent on the kinds of graphene dispersions. One may note that nonlinear graphene type results in greater resonance frequency compared to linear/uniform types. Therefore, dynamic behavior of a graphene based beam under thermal loads may be controlled employing a suitable distribution of graphene.

In Figs.6 and 7, forced vibration curves for graphene based beams have been depicted based on uniform and linear types of graphene dispersion. Linear temperature rise across the thickness has been assumed as ΔT=50. Increase of graphene weight fractions may lead to greater resonance frequency together with lower deflection before resonances zone. It means that the amplitude-frequency curves may move toward higher frequencies with enlargement of graphene amount. This highlights that the graphene based beams become more rigid and represent superior mechanical performances under dynamical loading. Accordingly, the resonances may be delayed via increase of graphene content. According to the graphs, one may find that nonlinear graphene type may lead to greatest resonance frequency than uniformly or linearly types. These observations are owning to highest structural rigidity of graphene based beams provided by nonlinear dispersion type. Therefore, dynamic behavior of a graphene based beam under mechanical-thermal loads may be controlled employing a suitable distribution for graphene.

Fig.8 depicts 1st mode shape for clamped graphene based beams based upon different graphene dispersion types at L=10h. Linear temperature rise across the thickness has been assumed as ΔT=50 and exerted harmonic loading has the external frequency as Ω=5. There are two important results in the presented graph. Firstly, nonlinear and linear graphene types respectively represent lowest and greatest dynamical amplitudes. Secondly, one may understand that dynamical amplitude based on all dispersion kinds is remarkably decreased via increase of graphene weight fractions.

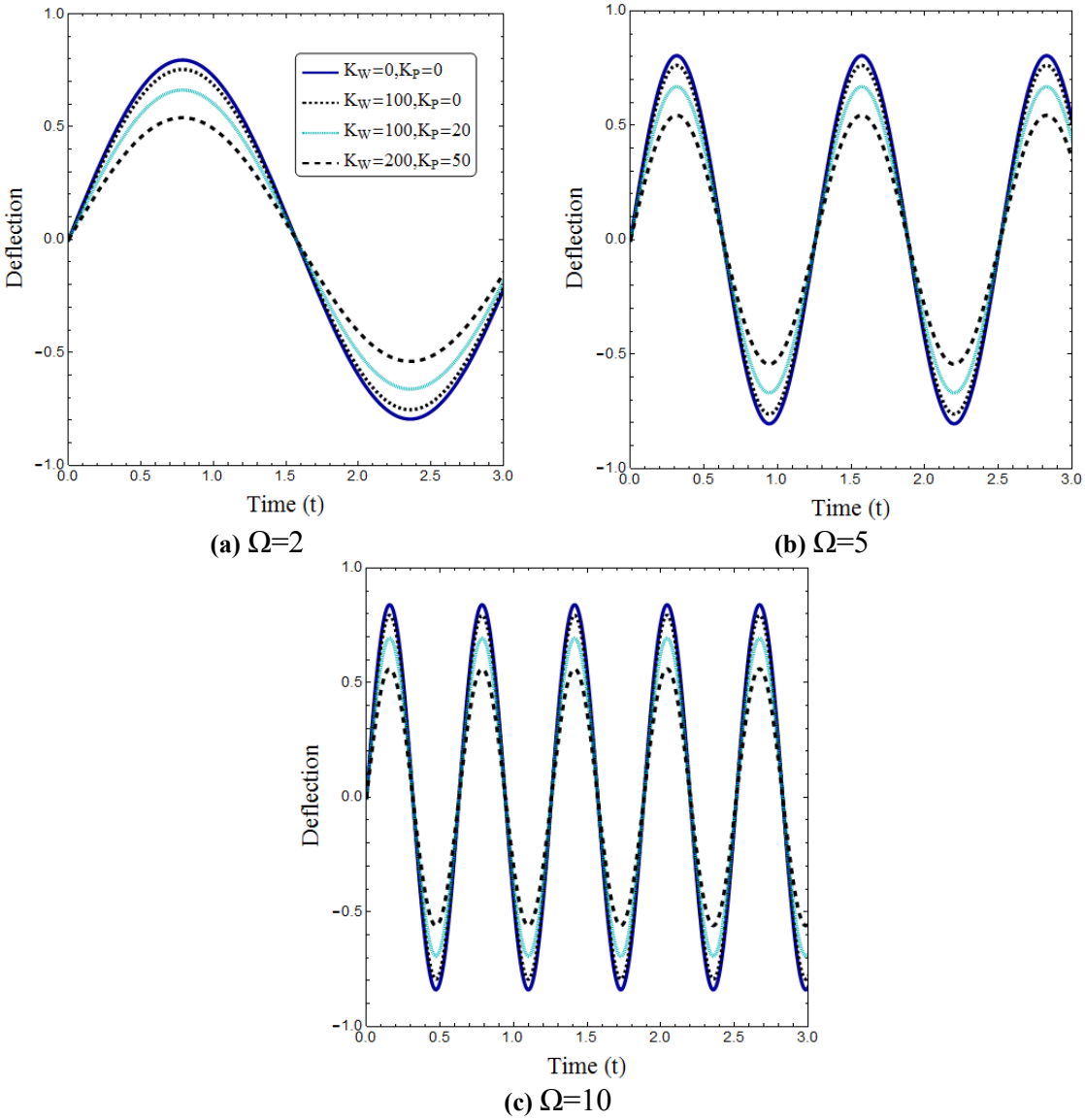

Fig. 9 Dynamic response of S-S nano-composite beam with uniform GPLs for various foundation parameters and excitation frequencies (L/h=10, W^*_{GPL}=1%, ΔT=50)

Another crucial factors for investigating dynamical behaviors of graphene based beams are external frequency (Ω) of exerted force together with foundation parameters which their impacts on time responses of graphene based beams have been depicted in Fig.9 at ΔT=50 K. Another deduction is that the graphene based beams experience larger numbers of oscillation within a particular time intervals by increasing in magnitude of external frequency. Furthermore, the dynamical amplitude is influenced by foundation parameters which are Winkler and Pasternak models. Enlargement of Winkler or Pasternak parameter will reduce the deflections of graphene based beams at every values of external frequencies.

6. Conclusions

In the present article, dynamic analysis of functionally graded (FG) graphene-reinforced beams under thermal loading was carried out based on finite element approach. The presented formulation was based on a higher order refined beam element accounting for shear deformations. The graphene-reinforced beam was exposed to transverse periodic mechanical loading. Graphene platelets had three types of dispersion within the structure including uniform-type, linear-type and nonlinear-type.

- Increase of graphene weight fractions led to greater resonance frequency together with lower deflection before resonances zone.
- It is well known that the beam structural rigidity will reduced via linear temperature rise. Accordingly, the forced vibration curves will move to the left highlighting smaller resonance frequency.
- Linear temperature rise impacts were dependent on the kinds of graphene dispersions.
- Nonlinear graphene type results in greater resonance frequency compared to linear/uniform types.

Acknowledgement

The authors would like to thank Mustansiriyah university (www.uomustansiriyah.edu.iq) Baghdad-Iraq for its support in the present work.

References

Ahankari, S. S and Kar, K. K. (2010), "Hysteresis measurements and dynamic mechanical characterization of functionally graded natural rubber–carbon black composites", *Polym. Eng. Sci.*, **50**(5), 871-877. https://doi.org/10.1002/pen.21601.

Al-Maliki, A. F., Faleh, N. M. and Alasadi, A. A. (2019), "Finite element formulation and vibration of nonlocal refined metal foam beams with symmetric and non-symmetric porosities", *Struct. Monitor Maintenance*, **6**(2), 147-159. https:// doi.org/10.12989/smm.2019.6.2.147.

Ahmed, R. A., Fenjan, R. M. and Faleh, N. M. (2019), "Analyzing post-buckling behavior of continuously graded FG nanobeams with geometrical imperfections", *Geomech. Eng.*, **17**(2), 175-180. https://doi.org/10.12989/gae.2019.17.2.175.

Barati, M. R. (2017), "Nonlocal-strain gradient forced vibration analysis of metal foam nanoplates with uniform and graded porosities", *Adv. Nano Res.*, **5**(4), 393-414. https://doi.org/10.12989/anr.2017.5.4.393.

Barati, M. R. and Zenkour, A. M. (2018), "Analysis of postbuckling of graded porous GPL-reinforced beams with geometrical imperfection", *Mech. Adv. Mater. Struct.*, **26**(6), 503-511. https://doi.org/10.1080/15376494.2017.1400622.

Bounouara, F., Benrahou, K. H., Belkorissat, I. and Tounsi, A. (2016), "A nonlocal zeroth-order shear deformation theory for free vibration of functionally graded nanoscale plates resting on elastic foundation", *Steel Compos. Struct.*, **20**(2), 227-249. https://doi.org/10.12989/scs.2016.20.2.227.

Esawi, A. M. K., Morsi, K., Sayed, A., Taher, M and Lanka, S. (2011), "The influence of carbon nanotube (CNT) morphology and diameter on the processing and properties of CNT-reinforced aluminium composites", *Compos. Part A Appl. Sci. Manufact.*, **42**(3), 234-243.

Faleh, N.M., Ahmed, R.A., and Fenjan, R.M. (2018), "On vibrations of porous FG nanoshells", *Int. J. Eng. Sci.*, **133**, 1-14. https://doi.org/10.1016/j.ijengsci.2018.08.007.

Fang, M., Wang, K., Lu, H., Yang, Y. and Nutt, S. (2009), "Covalent polymer functionalization of graphene nanosheets and mechanical properties of composites", *J. Mater. Chem.*, **19**(38), 7098-7105. https://doi.org/10.1039/B908220D.

Fenjan, R. M., Ahmed, R. A., Alasadi, A. A. and Faleh, N. M. (2019), "Nonlocal strain gradient thermal vibration analysis of double-coupled metal foam plate system with uniform and non-uniform porosities", *Coupl. Syst. Mech.*, **8**(3), 247-257. https://doi.org/10.12989/csm.2019.8.3.247.

Feng, C., Kitipornchai, S. and Yang, J. (2017), "Nonlinear free vibration of functionally graded polymer composite beams reinforced with graphene nanoplatelets (GPLs)", *Eng. Struct.*, **140**, 110-119. https://doi.org/10.1016/j.engstruct.2017.02.052.

Gojny, F. H., Wichmann, M. H. G., Köpke, U., Fiedler, B and Schulte, K. (2004), "Carbon nanotube-reinforced epoxy-composites: enhanced stiffness and fracture toughness at low nanotube content", *Compos. Sci. Technol.*, **64**(15), 2363-2371.

Keleshteri, M. M., Asadi, H. and Wang, Q. (2017), "Large amplitude vibration of FG-CNT reinforced composite annular plates with integrated piezoelectric layers on elastic foundation", *Thin-Walled Struct.*, **120**, 203-214. https://doi.org/10.1016/j.tws.2017.08.035.

King, J. A., Klimek, D. R., Miskioglu, I. and Odegard, G. M. (2013), "Mechanical properties of graphene nanoplatelet/epoxy composites", *J. Appl. Polym Sci.*, **128**(6), 4217-4223. https://doi.org/10.1002/app.38645.

Kitipornchai, S., Chen, D. and Yang, J. (2017), "Free vibration and elastic buckling of functionally graded porous beams reinforced by graphene platelets", *Mater. Design*, **116**, 656-665. https://doi.org/10.1016/j.matdes.2016.12.061.

Liew, K. M., Lei, Z. X. and Zhang, L. W. (2015), "Mechanical analysis of functionally graded carbon nanotube reinforced composites: A review", *Compos. Struct.*, **120**, 90-97. https://doi.org/10.1016/j.compstruct.2014.09.041.

Lin, F., Yang, C., Zeng, Q. H and Xiang, Y. (2018), "Morphological and mechanical properties of graphene-reinforced PMMA nanocomposites using a multiscale analysis", *Comput. Mater Sci.*, **150**, 107-120.

Mouffoki, A., Bedia, E. A., Houari, M. S. A., Tounsi, A. and Mahmoud, S. R. (2017), "Vibration analysis of nonlocal advanced nanobeams in hygro-thermal environment using a new two-unknown trigonometric shear deformation beam theory", *Smart Struct. Syst.*, **20**(3), 369-383. https://doi.org/10.12989/sss.2017.20.3.369.

Nieto, A., Bisht, A., Lahiri, D., Zhang, C and Agarwal, A. (2017), "Graphene reinforced metal and ceramic matrix composites: A review", *Mater. Rev.*, **62**(5), 241-302.

Rafiee, M. A., Rafiee, J., Wang, Z., Song, H., Yu, Z. Z. and Koratkar, N. (2009), "Enhanced mechanical properties of nanocomposites at low graphene content", *ACS nano*, **3**(12), 3884-3890. https://doi.org/10.1021/nn9010472.

Rezaiee-Pajand, M., Masoodi, A. R. and Mokhtari, M. (2018), "Static analysis of functionally graded non-prismatic sandwich beams", *Adv. Comput. Design*, **3**(2), 165-190. https://doi.org/10.12989/acd.2018.3.2.165.

She, G.L., Yan, K.M., Zhang, Y.L., Liu, H.B. and Ren, Y.R. (2018), "Wave propagation of functionally graded porous nanobeams based on non-local strain gradient theory", *Euro. Phys. J. Plus*, **133**(9), 368.

She, G. L., Jiang, X. Y. and Karami, B. (2019), "On thermal snap-buckling of FG curved nanobeams", *Mater. Res. Express*, **6**(11), 115008. https://doi.org/10.1088/2053-1591/ab44f1.

Shen, H. S., Xiang, Y., Lin, F. and Hui, D. (2017), "Buckling and postbuckling of functionally graded graphene-reinforced composite laminated plates in thermal environments", *Composites Part B Eng.*, **119**, 67-78. https://doi.org/10.1016/j.compositesb.2017.03.020.

Song, M., Kitipornchai, S. and Yang, J. (2017), "Free and forced vibrations of functionally graded polymer composite plates reinforced with graphene nanoplatelets", *Compos. Struct.*, **159**, 579-588. https://doi.org/10.1016/j.compstruct.2016.09.070.

Yang, B., Yang, J. and Kitipornchai, S. (2017). Thermoelastic analysis of functionally graded graphene reinforced rectangular plates based on 3D elasticity", *Meccanica*, **52**(10), 2275-2292. https://doi.org/10.1007/s11012-016-0579-8.

Zemri, A., Houari, M. S. A., Bousahla, A. A. and Tounsi, A. (2015), "A mechanical response of functionally graded nanoscale beam: an assessment of a refined nonlocal shear deformation theory beam theory", *Struct. Eng. Mech.*, **54**(4), 693-710. https://doi.org/10.12989/sem.2015.54.4.693.

Zhang, L.W. (2017), "On the study of the effect of in-plane forces on the frequency parameters of CNT-reinforced composite skew plates", *Compos. Struct.*, **160**, 824-837. https://doi.org/10.1016/j.compstruct.2016.10.116.

CC